Accepted Manuscript

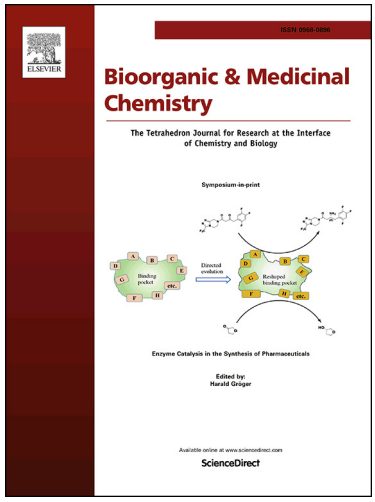

Discovery of (S)-6-methoxy-chroman-3-carboxylic acid (4-pyridin-4-yl-phenyl)-amide as potent and isoform selective ROCK2 inhibitors

Jinpeng Pan, Yan Yin, Lianhua Zhao, Yangbo Feng

PII: S0968-0896(19)30055-0
DOI: https://doi.org/10.1016/j.bmc.2019.02.047
Reference: BMC 14783

To appear in: *Bioorganic & Medicinal Chemistry*

Received Date: 10 January 2019
Revised Date: 15 February 2019
Accepted Date: 20 February 2019

Please cite this article as: Pan, J., Yin, Y., Zhao, L., Feng, Y., Discovery of (S)-6-methoxy-chroman-3-carboxylic acid (4-pyridin-4-yl-phenyl)-amide as potent and isoform selective ROCK2 inhibitors, *Bioorganic & Medicinal Chemistry* (2019), doi: https://doi.org/10.1016/j.bmc.2019.02.047

Graphical Abstract

To create your abstract, type over the instructions in the template box below.
Fonts or abstract dimensions.

Discovery of (S)-6-methoxy-chroman-3-carboxylic acid (4-pyridin-4-yl-phenyl)-amide as potent and isoform selective ROCK2 inhibitors

Leave this area blank for abstract info.

Jinpeng Pan[a], Yan Yin[a,*], Lianhua Zhao[a],Yangbo Feng[b,*]

[a]*School of Chemical and Environment Engineering, Shanghai Institute of Technology, 100 Hai Quan Rd., Shanghai, 201418, P. R. China*

[b]*Medicinal Chemistry, The Scripps Research Institute, 130 Scripps Way, Jupiter, Florida 33458, United States*

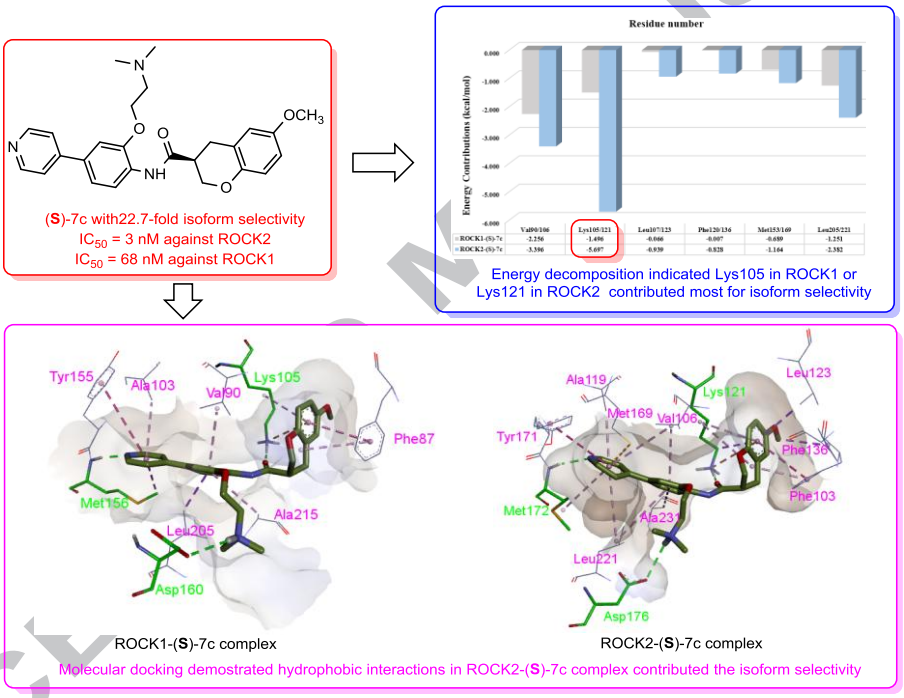

Bioorganic & Medicinal Chemistry
journal homepage: www.elsevier.com

Discovery of (S)-6-methoxy-chroman-3-carboxylic acid (4-pyridin-4-yl-phenyl)-amide as potent and isoform selective ROCK2 inhibitors

Jinpeng Pan[a], Yan Yin[a,*], Lianhua Zhao[a], Yangbo Feng[b,*]

[a] *School of Chemical and Environment Engineering, Shanghai Institute of Technology, 100 Hai Quan Rd., Shanghai, 201418, P. R. China*
[b] *Medicinal Chemistry, The Scripps Research Institute, 130 Scripps Way, Jupiter, Florida 33458, United States*

ARTICLE INFO

Keywords:
ROCK
Isoform selectivity
ROCK inhibitors
Chromans
Computational theoretical studies

ABSTRACT

ROCK1 and ROCK2 are highly homologous isoforms. Accumulated studies indicate that they have distinct different functions, and the development of isoform selective ROCK inhibitors will pave new roads for the treatment of various diseases. In this work, a series of amide-chroman derivatives were synthesized and biologically evaluated in order to develop potent and isoform selective ROCK2 inhibitors. Remarkably, (S)-6-methoxy-chroman-3-carboxylic acid (4-pyridin-4-yl-phenyl)-amide ((S)-**7c**) possessed ROCK2 inhibitory activity with an IC_{50} value of 3 nM and 22.7-fold isoform selectivity (vs. ROCK1). Molecular docking indicated that hydrophobic interactions were the key element for the high potency and isoform selectivity of (S)-**7c**. The binding free energies predicted by MM/GBSA were in good agreement with the experimental bioactivities, and the analysis of individual energy terms suggested that residue Lys105 in ROCK1 or Lys121 in ROCK2 was the key residue for the isoform selectivity of (S)-**7c**.

1. Introduction

Rho-associated kinases (ROCKs), originally identified as the effectors of small GTPase Rho, play a major role in mediating rearrangement of the actomyosin cytoskeleton.[1-5] Two ROCK isoforms, ROCK1 and ROCK2, have been identified in mammalian system. They have been shown to function independently of each other and play non-overlapping roles in cellular processes,[6-8] so selective inhibition of the two kinase isoforms can result in different biological effects on physiological and pathological processes. Recently, isoform selective inhibition of ROCK2 has been suggested to have wide applications in treating Alzheimer disease (AD),[9-11] Parkinson's disease (PD),[12] vascular diseases,[13] focal cerebral ischemia,[14] and neuroblastoma.[15] In addition, the hypertensive effects of systemic ROCK inhibition are speculated to be mainly due to ROCK1 inhibition.[16] Therefore, isoform selective ROCK2 inhibitors might provide medications with less safety concerns. However the two isoforms share an overall 65% homology in amino acid sequence and 92% homology in kinase domain,[17] and most small-molecule ROCK inhibitors cannot distinguish between the two kinases, resulting in non-isoform-selective pharmacological inhibition. Although significant efforts have been applied to develop isoform selective ROCK inhibitors, few high-subtype selective ROCK inhibitors were publicly reported over the past decade.[18-21] Therefore, the discovery of isoform-selective ROCK inhibitors remains a great challenge due to the high conservation and similarity between the two homologous kinase isoforms.

SR3677, one of the best known ATP-competitive ROCK inhibitors, demonstrated an approximately 17.5-fold isoform selectivity of ROCK 2 over ROCK1 (IC_{50} = 3.2 nM against ROCK2, and 56 nM against ROCK1, **Figure 1**).[22] Investigation into Alzheimer's disease (AD) mouse models with **SR3677** suggested ROCK inhibition reduced Aβ levels through independent mechanisms, and the potential for isoform-selective ROCK inhibitors to combat Aβ production for the treatment of AD raised considerable enthusiasm.[23] Molecular docking study indicated the hydrophobic interaction of the benzodioxane phenyl ring in **SR3677** with the hydrophobic surface of hydrophobic pocket in ROCKs is the dominating factor that contributes to the high inhibitory potency of **SR3677** against ROCK2. [22] To our delight, modifications on the benzodioxane group as well as the bottom pyrazol group of **SR3677** (**Figure 1**) led to (S)-6-methoxy-chroman-3-carboxylic acid (4-pyridin-4-yl-phenyl)-amide ((S)-**7c**) which has ROCK2 inhibitory potency of IC_{50}= 3 nM and up to 22.7-fold isoform selectivity against ROCK1. Modeling studies including molecular docking, molecular dynamics simulations demonstrated that the difference of hydro-

*Corresponding authors. (86)-21-6087-7220. E-mail: yinyan@sit.edu.cn (To Yan Yin)

*Corresponding authors. 561-909-9820. E-mail: yangbof@gmail.com (To Yangbo Feng)

that the difference of hydrophobic contacts formed in ROCK1 and ROCK2 could be the main reason for the generation of isoform selectivity and residue Lys105 in ROCK1 or Lys121 in ROCK2 played a key role in isoform selectivity. Herein, the discovery of (S)-7c as a potent and isoform selective ROCK2 inhibitor including synthesis, in vitro activity evaluation, and computational studies will be reported in detail.

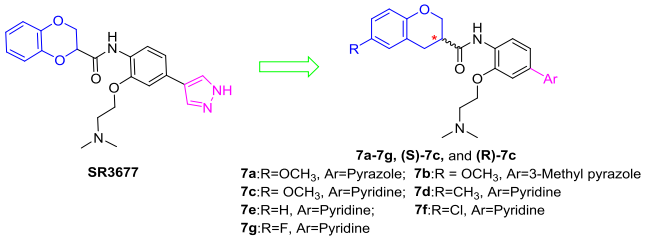

Figure 1. New ROCK inhibitors.

2. Results and discussion

Cyclization of 3-substituted salicaldehydes **1** with acrylonitrile in the presence of equivalent DABCO, followed cyano hydrolysis gave chromene acids **2**. Then hydrogenation of **2** provided chroman-3-carboxylic acids **3** in high yields **(**Scheme 1).

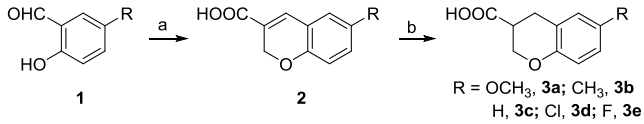

Scheme 1. Reagents and conditions: (a) (i) Acrylonitrile, DABCO, 110°C; (ii) NaOH, H2O, reflux; (b) H2, 10% Pd/C, methanol, rt.

Although optical 3-methoxyl chroman-3-carboxylic acids can be obtained by chiral auxiliaries or metal-catalyzed asymmetric hydrogenation,[24] the chiral auxiliary method can only provide sub-gram quantities of each enantiomer as well as the need for expensive selectride. In asymmetric hydrogenation environment-tally unfriendly metal catalysts and expensive chiral ligands were used. To overcome the above shortcomings, a cheap and green synthesis method was developed in the preparation of optical **3a** from racemic **3a**. Both **(*R*)-3a** and **(*S*)-3a** were obtained with more than 95% enantiomeric excess (ee) *via* salification with (1R,2R) or (1S,2S) 2-amino-1-(4-nitrophenyl)-propane-1,3-diol, recrystalli-zation in CH_3CN/CH_3OH, dissociation with HCl, and recrystalli-zation in Hexane/CH_3CN. Both (1R, 2R) and (1S, 2S) chiral resolving agents can be recovered after a series of treatment of the crystal or mother liquor including acidification, extraction, alkalization of aqueous phase, and extraction, etc. (Figure 2).[25-27]

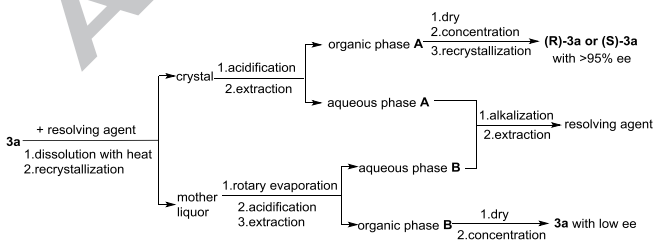

Figure 2. Preparation of (R)-3**a** and (S)-3**a** from racemic 3**a**.

Nucleophilic substitution reaction between commercially available 4-bromo-2-fluoro-nitrobenzene and 2-dimethylamino-ethanol, followed by Suzuki coupling gave nitro intermediates **5**. Then **5** were reduced to aniline derivatives **6** with stannous chloride. Amide formation reaction between acids **3**, (S)-**3**, or (R)-**3** and **6** produced the desired compounds **7a-7g,** (S)-**7c**, and (R)-**7c** with HATU as the coupling reagent and DIEA as the organic base (Scheme 2).

Inhibitory activities against ROCK1 and ROCK2 of all synthesized compounds (**7a-7g,** (S)-**7c**, and (R)-**7c**) were evaluated and presented in Table 1 as IC_{50} values. Effects of bottom aromatic groups on the inhibition and isoform selectivity were initially investigated. Compound **7a** (**SR3850**) with a pyrazole group displayed strong inhibition toward both ROCK isoforms (IC_{50} = 3.4nM for ROCK1, and 0.7nM for ROCK2) and poor isoform selectivity (4.8 fold).[28] Compound **7b** with the 3-methyl-1H-pyrazole group had single digital nM potency against ROCK2 (IC_{50} = 1.2nM) and IC_{50} = 16.3nM value against ROCK1 so as to improve isoform selectivity compared with **7a** (13.6 fold for **7b** vs 4.8 fold for **7a**). Most encouraging was the finding that inhibitor **7c** with a pyridine group as the hinge binding moiety had a significant drop in ROCK1 potency (IC_{50} = 170nM against ROCK1 and 9nM against ROCK2), thus resulting in an 18.9 fold isoform selectivity. The SAR from the hinge binding region indicated that replacement of pyrazole with pyridine might significantly weaken ROCK1 inhibitory activity while still retaining excellent ROCK2 potency thus yielding higher isoform selectivity.

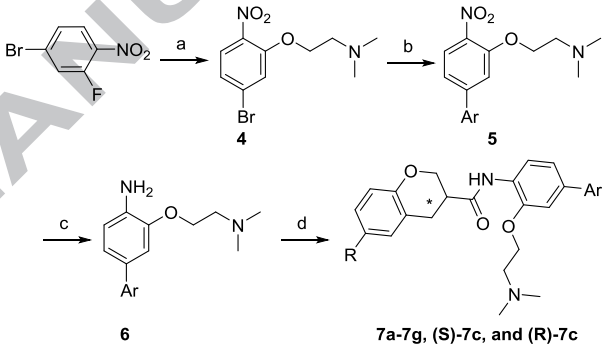

Scheme 2. Reagents and conditions: (a) 2-Dimethylamino-ethanol, NaH, THF, rt; (b) Ar-boronic acid pinacol ester or Ar-boronic acid, $Pd(PPh_3)_4$, Na_2CO_3, dioxane, H_2O, 100°C; (c) $SnCl_2$, EtOAc, rt;(d) **3**, **(S)-3a**,or **(R)-3a**, HATU, DIEA, DMF, rt.

The SAR information of substitutions at the C6 position of the chroman ring was then studied. Compared with **7c**, compounds **7d** (with a 6-CH_3) and **7f (**with a 6-Cl) showed similar ROCK1 inhibition and around 4 times weaker ROCK2 inhibition (IC_{50} = 169 nM against ROCK1, 24 nM against ROCK2 for **7d**; 135 nM against ROCK1, 22 nM against ROCK2 for **7f**). **7e** (with no 6-substitution) had a similar ROCK2 inhibitory activity and better ROCK1 inhibition (IC_{50} = 30 nM against ROCK1, 7 nM against ROCK2), and **7g** (with a 6-F group) exhibited a little higher ROCK1 inhibition (IC_{50} = 104 nM) while retaining the same ROCK2 potency (IC_{50} = 7 nM). SAR information of substitutions at the C6 position of the chroman ring suggested that a 6-methoxyl group would be less tolerated for ROCK1 inhibition and consequently produced better isoform selectivity.

Molecules with a chiral center have two enantiomers.[29] Although the physical and chemical properties of the two isomers are the same, the pharmacological activities needs rewording because of stereoselective reactions at the binding sites. Due to the high ROCK2 inhibitory activity and impressive isoform selectivity of **7c**, it was chosen to probe possible stereochemical preferences and the influence of chirality on isoform selectivity. As shown in entries 8 and 9 of Table 1, (S)-**7c** showed 22.7-fold isoform selectivity with IC_{50} = 68 nM against ROCK1 and 3 nM against ROCK2 inhibitory activities, while (R)-**7c** had only 3-fold isoform selectivity and weaker inhibitory activities toward

Table 1. The chemical structures and inhibitory activities

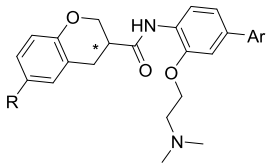

7a-7g, (S)-7c, and **(R)-7c**

Entry	Compd.	R	Ar	ROCK1 IC_{50} (nM)[a]	ROCK2 IC_{50} (nM)[a]	Selectivity
1	**7a (SR3850)**	OCH_3	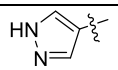	3.4	0.7	4.8
2	**7b**	OCH_3	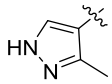	16.3	1.2	13.6
3	**7c**	OCH_3	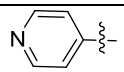	170	9	18.9
4	**7d**	CH_3	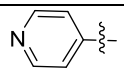	169	24	7.0
5	**7e**	H	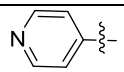	30	7	4.3
6	**7f**	Cl	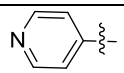	135	22	6.1
7	**7g**	F	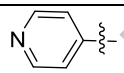	104	7	14.8
8	(S)-**7c**	OCH_3	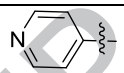	68	3	22.7
9	(R)-**7c**	OCH_3		523	172	3.0

[a] Values are means of three or more experiments. The error in these values is within ±30% of mean.

both ROCK1 and ROCK2 kinases (IC_{50} = 523 nM against ROCK1, 172 nM against ROCK2). These results suggested that the S configuration was stereochemically preferred for both ROCK inhibition and isoform-selectivity among this series of compounds.

Molecular docking is one of the most frequently used methods in drug discovery due to its ability to predict the binding-interactions between ligand and protein.[30,31] To explain the inhibitory activity and isoform selectivity variation between the two enantiomers of **7c**, (S)-**7c** and (R)-**7c** were docked into the active sites of ROCK1 (PDB: 2ETR) and ROCK2 (PDB: 4L6Q) using the Surflex-Dock program and their binding behaviors in the ligand-protein complexes were predicted from the amino acid residue level (Figure 3). Comparison of the (S)-**7c**-ROCK1 complex**,** the (S)-**7c**-ROCK2 complex, the (R)-**7c**-ROCK1 complex, and the (R)-**7c**-ROCK2 complex, showed that the binding poses of one compound at the binding site of either ROCK1 or ROCK2 was quite similar, while binding poses of (S)-**7c**-protein complex and (R)-**7c**-protein complex were obviously different.

The hydrogen bond interactions in the above four enzyme-ligand complexes were the same: the first one is between the amide carbonyl and Lys105 in ROCK1 or Lys 121 in ROCK2; the second is between the protonated $(CH_3)_2N$ and Asp160 in ROCK1 or Asp 176 in ROCK2, and the third is between the pyridine N and Met156 in ROCK1 or Met 172 in ROCK2, this clearly explains why both (S)-**7c** and (R)-**7c** were potent against both ROCK1 and ROCK2.

Hydrophobic interactions can be subdivided into pi-hydrophobic interaction, alkyl hydrophobic interaction, and mixed pi/alkyl hydrophobic interaction, which were shown as deep pink, pink, and faded pink, respectively. Electronic interactions and hydrophobic interactions in these systems were quite different. In the (S)-**7c**-ROCK1 complex, there was one electronic interaction between chrome and Lys105, and nine hydrophobic interactions (Ala103-C⋯pyridine ring, Tyr155-phenyl ring⋯pyridine ring, Met156-C⋯pyridine ring, Leu205-C⋯middle phenyl ring, Lys105-C⋯phenyl ring in chroman, Val90-C⋯middle phenyl ring, Ala215-C⋯middle phenyl ring, Phe87-phenyl ring⋯pyran ring, and Phe87-phenyl ring⋯phenyl ring in chroman). In the (S)-**7c**-ROCK2 complex, there was one electronic interaction between chroman and Lys121, and thirteen hydrophobic interactions (Ala119-C⋯pyridine ring, Met169-C⋯pyridine ring, Tyr171- phenyl ring⋯pyridine ring, Met172-S⋯pyridine ring, Leu221-C⋯pyridine ring, Leu221-C⋯middle phenyl ring, Ala231-C⋯middle phenyl ring, Val106-C⋯pyridine ring, Val106-C⋯middle phenyl ring, Lys121-C⋯pyran ring, Lys121-C⋯phenyl ring in chroman, Phe103-phenyl ring⋯pyran ring, Phe103-phenyl ring⋯phenyl ring in chroman, Leu123-C⋯phenyl ring in chroman, and Phe136-phenyl ring⋯phenyl ring in chroman). In the (R)-**7c**-ROCK1 complex, there were five hydrophobic interactions (Ala103-

C⋯pyridine ring, Leu205-C⋯middle phenyl ring, Leu205-C⋯pyridine ring, Val90-C⋯middle phenyl ring, and Ala215-C⋯middle phenyl ring). In the (R)-**7c**-ROCK2 complex, there were five hydrophobic interactions (Ala119-C⋯pyridine ring, Leu221-C⋯phenyl ring, Leu221-C⋯pyridine ring, Ala231-C⋯middle phenyl ring, and Val106-C⋯middle phenyl ring).

We believed that the number of amino acids involved in the binding, electronic interactions and hydrophobic interactions between the ligand and protein contributed to the higher inhibitory activities of (S)-**7c** against ROCK isoforms than (R)-**7c**. At the same time hydrophobic interactions in the (S)-**7c**-ROCK2 complex (Met169-C⋯pyridine ring, Leu221-C⋯pyridine ring, Val106-C⋯pyridine ring, Lys121-C⋯pyran ring, Leu123-C⋯phenyl ring in chroman, Phe136-phenyl⋯phenyl ring in chroman) may contribute the isoform selectivity of (S)-configuration of **7c**.

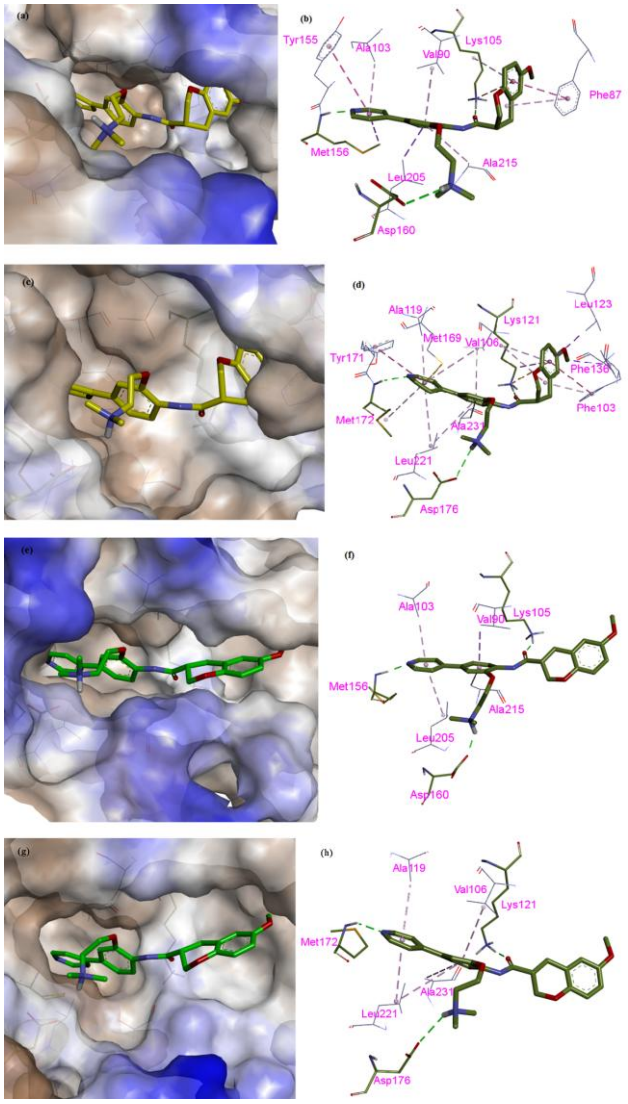

Figure 3. Docking results. **(a)** 3D schematic view of **(S)-7c**-ROCK1 complex; **(b)** 2D schematic view of **(S)-7c**-ROCK1 complex; **(c)** 3D schematic view of **(S)-7c**-ROCK2 complex; **(d)** 2D schematic view of **(S)-7c**-ROCK2 complex; **(e)** 3D schematic view of **(R)-7c**-ROCK1 complex; **(f)** 2D schematic view of **(R)-7c**-ROCK1 complex; **(g)** 3D schematic view of **(R)-7c**-ROCK2 complex; **(h)** 2D schematic view of **(R)-7c**-ROCK2 complex. Hydrogen bonds, hydrophobic interactions and electrostatic interactions were shown as green, pink and orange dotted lines, respectively.

In order to evaluate the reliability of the docking results, the (S)-**7c**-ROCK1 complexes and (S)-**7c**-ROCK2 complexes were submitted to the studies for molecular dynamics (MD) simulation studies with the structures shown in Figure 3 as the initial structures. As shown in Figure 4, both complexes reached a stabilization at 10 ns with subtle rmsd values (around 1.5Å, Figure 4**a**). The initial and final pharmacophore structures and other structures were basically similar (Figure 4**b** and 4**c**). As a result it could be inferred that the docking results were reliable.

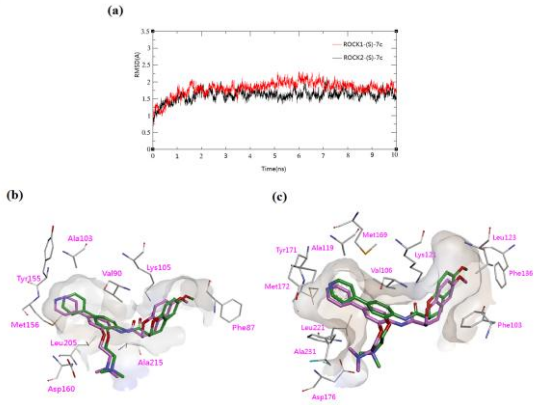

Figure 4. Molecular dynamics simulation. **(a)** Plot of RMSD versus time. **(b)** (S)-**7c**-ROCK1 complex. **(c)** (S)-**7c**-ROCK2 complex. The initial and final structures are represented in green and magenta, respectively.

The predicted binding free energy (ΔG_{bind}) can give a good explanation of the activity difference between the studied inhibitors.[32] The binding free energies of both the ROCK1-(S)-**7c** and ROCK2-(S)-**7c** complexes were predicted by the Molecular Mechanics/Generalized Born Surface Area (MM/GBSA) method in Amber using 50 snapshots extracted from 5 to 10 ns. At the same time, individual energy components of the binding free energies including van der Waals contribution (ΔG_{vdw}), electrostatic contribution (ΔG_{ele}), the polar contribution to solvation free energy (ΔG_{GB}), and the non-polar contribution to solvation free energy (ΔG_{SA}) were also calculated (Table 2). ΔG_{vdw}, ΔG_{ele}, ΔG_{GB}, ΔG_{SA}, and ΔG_{bind} were -52.22 kcal mol^{-1}, -55.02 kcal mol^{-1}, 64.19 kcal mol^{-1}, -7.25 kcal mol^{-1}, and -50.30 kcal mol^{-1} in ROCK1-(S)-**7c**, and -60.01 kcal mol^{-1}, -55.68 kcal mol^{-1}, 65.54 kcal mol^{-1}, -7.66 kcal mol^{-1}, and -57.81 kcal mol^{-1} in ROCK2-(S)-**7c**, respectively.

According to the predicted energies, the following conclusions can be drawn: (a) In both systems, $\Delta G_{vdw,}$ ΔG_{ele} and ΔG_{SA} were favorable, and ΔG_{GB} was unfavorable for the binding and inhibitory activities. (b) The differences of ΔG_{ele}, ΔG_{GB}, and ΔG_{SA} between the two systems were subtle. (c) The calculated ΔG_{bind} value of the ROCK2-(S)-**7c** complex was lower than the ROCK1-(S)-**7c** complex, indicating that (S)-**7c** had a higher potency to ROCK2 than to ROCK1, which was in good agreement with the experimental activities (IC_{50} = 3 nM against ROCK2 and 68 nM against ROCK1). (d) Usually, the van der Waals energy is closely correlated to the hydrophobic interactions, ΔG_{vdw} value of the ROCK2-(S)-**7c** complexes was significantly lower compared with the ROCK1-(S)-**7c** complexes. So it was hypothesized that the hydrophobic interactions formed in the protein-(S)-**7c** complexes played a key role in the isoform selectivity of ROCK kinases, which was consistent with the docking results.

Table 2. The predicted binding free energies and individual energy components[a]

System		ROCK1-(S)-7c	ROCK2-(S)-7c
ΔG_{vdw}	Ave.	-52.22	-60.01
	Std.Dev.	1.30	1.84
ΔG_{ele}	Ave.	-55.02	-55.68
	Std.Dev.	4.26	4.18
ΔG_{GB}	Ave.	64.19	65.54

	Std.Dev.	3.63	2.99
ΔG_{SA}	Ave.	-7.25	-7.66
	Std.Dev.	0.14	0.09
ΔG_{bind}	Ave.	-50.30	-57.81
	Std.Dev.	2.04	2.09

[a] All energies are in kcal mol^{-1}.

Docking studies indicated that Val106, Lys121, Leu123, Phe136, Met169, and Leu221 had different interactions in the two ROCK isoforms. To further investigate the protein-ligand interactions, the energy contributions of these residues[33] were calculated and listed in Figure 5. In the ROCK2-**(S)-7c** complexes, the energy differences were 1.140, 4.201, 0.873, 0.820, 0.474, 1.131kcal/mol (Energy contributions of Val106, Lys121, Leu123, Phe136, Met169, and Leu221 were -3.396, -5.697, -0.939, -0.828, -1.164, and -2.382 kcal/mol in the ROCK2-**(S)-7c** complexes, respectively, and -2.256, -1.496, -0.066, -0.007, -0.689, and -1.251 kcal/mol in the ROCK1-**(S)-7c** complexes, respectively). Energy decomposition demonstrated residue Lys105 in ROCK1 or Lys121 in ROCK2 was the largest contribution to the isoform selectivity.

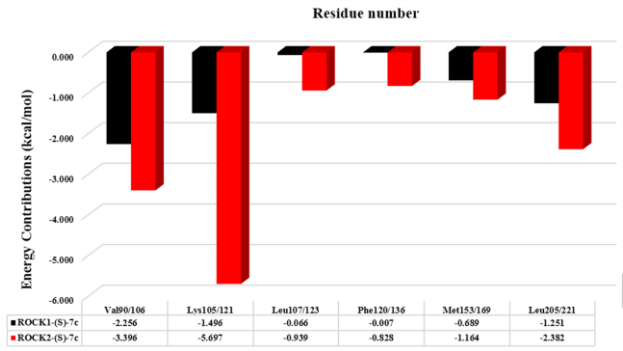

Figure 5. Contribution of key residues

3. Conclusion

In summary, a series of amide-chromans were synthesized and biologically evaluated in order to develop potent and isoform selective ROCK2 inhibitors. Remarkably, compound (S)-**7c,** which had a pyridyl group as the hinge-binding group exhibited high potency at ROCK2 with 22.7-fold isoform selectivity. Docking (S)-**7c** into the active site of ROCK1 and ROCK2 kinases provided insights in the binding features and demonstrated that the differences of hydrophobic interactions formed in ROCK1 and ROCK2 kinases were the main reason for the generation of isoform selectivity. MD simulations further verified the docking results. The inhibitory activities of (S)-**7c** against ROCK1 and ROCK2 were further backed by binding free energy analysis. The free energy deposition studies highlighted that residue Lys 105 in ROCK1 or Lys121 in ROCK2 play a key role in the isoform selectivity. These results deepen our understanding of the differences of hydrophobic region within ROCK1 and ROCK2, and facilitate the development of more isoform selective ROCK2 inhibitors. More biological data, such cellular activity, and pharmacokinetics in vitro and in vivo, will be reported in due course.

4. Experimental Section

Commercially available reagents and anhydrous solvents were used without further purification unless otherwise specified. Thin layer chromatography (TLC) analysis was performed on 1 mm thick precoated silica plates with ethyl acetate/hexane or methanol/dichloromethane as eluent. Column chromatography was performed on silica gel (200-300 Mesh) with ethyl acetate/hexane or methanol/dichloromethane as eluent. Chiral analytical HPLC analyses were performed with a Chiralpak® IF column (5μm, 4.6mm*250mm) and UV detection in 292 nm. The solvents used on the mobile phase were hexane and isopropanol. NMR spectra were recorded with a Bruker 500 MHz spectrometer. The high-resolution mass spectra (HRMS electrospray ionization) were performed with Solaril X70 FT-MS apparatus. The IR spectra were recorded on a Nicolet 6700 FT-IR spectrometer in the range of 400-4000 cm^{-1}. The melting points were measured on a SGW X-4 melting point instrument. Optical rotations were measured using a SGW®-1 automatic polarimeter. All compounds were determined to be >95% pure by analytical HPLC on Agilent technologies 1200 series with CH_3CN (solvent B)/H_2O+0.9%CH_3CN+0.1%TFA(solvent A) as eluents.

4.1. Synthesis procedure of compounds 7a-7g, (S)-7c and (R)-7c

1,4-Diazabicyclo[2,2,2]octane (DABCO, 17.5 mmol) was added to a solution of 2-hydroxy-benzaldehyde derivative (**1**, 17.5 mmol) in acrylonitrile (20 mL) . The mixture was refluxed under argon until **1** was completely conversed. The reaction mixture was cooled, and washed with 10% aqueous NaOH and ether. The organic phase was collected and concentrated under reduced pressure to give the intermediate nitrile.

The nitrile was added to 10% NaOH solution and the reaction mixture was heated at 60 ^{O}C until the complete disappearance of nitrile. Then the mixture was extracted with ether and the water phase was acidified with concentrated HCl, and extracted with ether (20 mL X 3). The combined organic phases were collected, washed with saturated NaCl, dried over anhydrous Na_2SO_4, and concentrated under vacuum to produce chromene -3-carbozylic acid **2**.

10% palladium on carbon (20 mg) was added to a mixture of chromene-3-carbozylic acid **2** (0.6 mmol) in methanol (5 mL). The mixture was stirred under a hydrogen atmosphere for 20 h at room temperature. After removal of the catalyst by filtration, the filtrate was concentrated in vacuo and purified by flash column chromatography to produce chroman-3-carboxylic acid **3a-3e.**

Racemic 6-methoxychroman-3-carboxylic acid (**3a**, 15 mmol) was dissolved in acetonitrile (300 mL) and the solution was warmed to reflux. (1S, 2S)-2-amino-1-(4-nitrophenyl)propane-1,3-diol (15 mmol) was added in one portion and the mixture was stirred at gentle reflux for 30 min. Methanol was then added dropwise until the solution became completely clear. The mixture was then allowed to crystallize at ambient temperature overnight. The precipitate was collected by filtration, washed with MeCN, and dried to afford a salt. Then this salt was treated with ethyl acetate (100 mL) and water (100 mL), acidified with 6 M aqueous HCl (10 mL), and stirred for 10 min. The organic layer was separated and washed with water (100 mL), dried over Na_2SO_4, and concentrated to dryness to obtain (S)-**3a**. Finally, the obtained (S)-**3a** was then recrystallized with hexane/ethyl acetate to produce (S)-**3a** in 36% yield and 97.1% ee (mobile phase: isopropanol/hexane/TFA = 50 mL: 50 mL: 0.5mL).

(R)-6-methoxychroman-3-carboxylic acid ((R)-**3a**) was prepared in 37% yield and 95.6% ee with the synthesis procedure of (S)-**3a** from racemic 6-methoxychroman-3-carboxylic acid and (1R, 2R)-2-amino-1-(4-nitrophenyl)propane-1,3-diol. (mobile phase: isopropanol/hexane/TFA = 50 mL:50 mL:0.5 mL).

4-Bromo-2-fluoro-1-nitrobenzene (**4**) (1.00 mmol) was added to a mixture of NaH (60% oil dispersion, 1.2 mmol) and 2-dimethylamino-ethanol (1.04 mmol) in THF (15 mL) at 0℃.The resulting mixture was allowed to warm to room temperature and stirred overnight. The solvent was removed by rotary evaporation and the obtained residue was partitioned between saturated aqueous $NaHCO_3$ (20 mL) and ethyl acetate (20 mL). The

aqueous layer was further extracted with ethyl acetate (3x20 mL) and the combined organic layers were washed with brine (30 mL), dried over Na_2SO_4, filtered, and concentrated to dryness. Without further purification, the bromide residue was dissolved in a mixture of dioxane and water (4:1, 10 mL). Then boronic acid pinacol ester or boronic acid (1.5 mmol), 2M K_2CO_3 (3.00 mmol), and tetrakis (triphenyphosphine) palladium (0.05mmol) were added to the mixture. Under argon protection, the reaction mixture was refluxed until the complete conversion of the bromide. After removal of the solvent under reduced pressure, the obtained residue was extracted with ethyl acetate (3 x 10 mL). The combined organic layers were dried, concentrated under reduced pressure, and purified by flash column chromatography to give intermediate **5**.

$SnCl_2$ (3 mmol) was added to a mixture of **5** (0.7 mmol) in ethyl acetate (5 mL) at room temperature. After the complete conversion of **5** detected by TLC, the reaction mixture was cool to 0 ^oC. Then $Na_2SO_4 \cdot 12H_2O$ was added slowly with strong magnetic stirring. Upper organic phase was filtrated, washed with saturated aqueous $NaHCO_3$ and saturated aqueous NaCl, dried with anhydrous Na_2SO_4, filtered, concentrated under reduced pressure, and purified by flash column chromatography to give aniline **6**.

Racemate or optically pure acid **3** (0.12 mmol), HATU (0. 1mmol), and DIEA (0.1 mmol) were added to the mixture of aniline **6** (0.1mmol) in DMF (2 mL). The resulting mixture was stirred at room temperature until **6** was completed conversed. Then the reaction mixture was concentrated under reduced pressure, extracted with ethyl acetate (2 X 20 mL). The combined organic phases were washed with brine (5 mL), dried over Na_2SO_4, filtered, concentrated to dryness, and purified by flash column chromatography to provide targeted compounds **7a-7g,** (S)-**7c** and (R)-**7c**.

*4.1.1. N-(2-(2-(Dimethylamino)ethoxy)-4-(pyrazol-4-yl)phenyl)-6-methoxychromane-3-carboxamide (**7a**).*

Yellow solid: 46% yield over four steps. Mp: 63-65°C. ^{1}H NMR (500 MHz, DMSO-d_6) δ 9.58 (NH, br, 1H), 8.06 (s, 2H), 7.88 (d, J = 8.5 Hz, 1H), 7.35 (s, 1H), 7.20 (d, J = 8.0 Hz, 1H), 6.73-6.68 (m, 3H), 4.38 (d, J = 10.0 Hz, 1H), 4.19 (t, J = 5.0 Hz, 2H), 3.96 (t, J = 10 Hz, 1H), 3.69 (s, 3H), 3.11-3.02 (m, 2H), 2.94-2.91 (m, 1H), 2.66 (t, J = 5.0 Hz, 2H), 2.27 (s, 6H); ^{13}C NMR (125 MHz, DMSO-d_6) δ 170.62, 153.54, 149.91, 148.15, 130.26, 126.58, 122.95, 122.27, 121.41, 118.19, 117.22, 116.88, 114.61, 113.78, 113.29, 111.66, 68.16, 67.63, 58.07, 55.82, 45.85, 28.33, 25.43. IR (KBr, cm^{-1}): 2919, 1674, 1596, 1530, 1498, 1211, 1040, 843. HRMS calcd for $C_{24}H_{29}N_4O_4$: 437.2183 [M+H^+], found 437.2184.

*4.1.2. N-(2-(2-(Dimethylamino)ethoxy)-4-(3-methyl-1H-pyrazol-4-yl)phenyl)-6-methoxychromane-3-carboxamide (**7b**).*

Yellow solid: 42% yield over four steps. Mp: 110-112°C. ^{1}H NMR (500 MHz, DMSO-d_6) δ 9.65 (NH, br, 1H), 7.92 (d, J = 8.0 Hz, 1H), 7.79 (s, 1H), 7.14 (s, 1H), 7.03 (d, J = 8.5 Hz, 1H), 6.74-6.68 (m, 3H), 4.38 (d, J = 10.0 Hz, 1H), 4.17 (t, J = 5.0 Hz, 2H), 3.96 (t, J = 10.0 Hz, 1H), 3.69 (s, 3H), 3.13-3.10 (m, 1H), 3.07-3.02 (m, 1H), 2.96-2.90 (m, 1H), 2.66 (t, J = 5.0 Hz, 2H), 2.38 (s, 3H), 2.26 (s, 6H); ^{13}C NMR (125MHz, DMSO-d_6) δ 170.71, 153.53, 149.68, 148.14, 131.05, 126.39, 122.87, 122.27, 119.69, 118.65, 117.22, 116.59, 114.59, 113.77, 113.05, 109.73, 74.02, 67.99, 67.64, 58.01, 55.80, 45.77, 28.33, 25.42. IR (KBr, cm^{-1}): 2928, 1679, 1595, 1532, 1498, 1211, 1041, 843. HRMS calcd for $C_{25}H_{31}N_4O_4$: 451.2340 [M+H^+], found 451.2332.

*4.1.3. N-(2-(2-(Dimethylamino)ethoxy)-4-(pyridine-4-yl)phenyl)-6-methoxychromane-3-carboxamide (**7c**).*

Yellow solid: 44% yield over four steps. Mp: 68-70°C. ^{1}H NMR (500 MHz, DMSO-d_6) δ 9.73 (NH, br , 1H), 8.61 (s, 2H), 8.14 (d, J = 8.0 Hz, 1H), 7.75 (d, J = 6.0 Hz, 2H), 7.55 (s, 1H), 7.44 (d, J = 8.5 Hz, 1H), 6.74-6.68 (m, 3H), 4.39 (d, J = 10.5 Hz, 1H), 4.26 (t, J = 5.0 Hz, 2H), 3.98 (t, J = 10.0 Hz, 1H), 3.69 (s, 3H), 3.21-3.15 (m, 1H), 3.08-3.03 (m, 1H), 2.97-2.92 (m, 1H), 2.68 (t, J = 5.0 Hz, 2H), 2.27 (s, 6H); ^{13}C NMR (125 MHz, DMSO-d_6) δ 171.06, 153.55, 150.58, 149.64, 148.13, 146.88, 133.58, 129.88, 122.43, 122.21, 121.39, 120.07, 117.24, 114.59, 113.80, 112.95, 68.26, 67.55, 66.82, 58.02, 55.81, 45.83, 28.28. IR (KBr, cm^{-1}): 2926, 1683, 1595, 1527, 1497, 1211, 1041, 811. HRMS calcd for $C_{26}H_{30}N_3O_4$: 448.2231 [M+H^+], found 448.2246.

*4.1.4. (S)-N-(2-(2-(Dimethylamino)ethoxy)-4-(pyridin-4-yl)phenyl)-6-methoxychromane-3-carboxamide((S)-**7c**).*

$[\alpha]_D^{20}$ = +10.42 (c = 0.45, $CHCl_3$).

*4.1.5. (R)-N-(2-(2-(Dimethylamino)ethoxy)-4-(pyridin-4-yl)phenyl)-6-methoxychromane-3-carboxamide((R)-**7c**).*

$[\alpha]_D^{20}$ = -6.83 (c = 0.34, $CHCl_3$).

*4.1.6. N-(2-(2-(Dimethylamino)ethoxy)-4-(pyridine-4-yl)phenyl)-6-methylchromane-3-carboxamide(**7d**).*

White solid: 40% yield over four steps. Mp: 187-189°C. ^{1}H NMR (500 MHz, DMSO-d_6) δ 9.69 (NH, br, 1H), 8.62 (d, J = 4.5 Hz, 2H), 8.12 (d, J = 8.0 Hz, 1H) 7.75 (d, J = 5 Hz, 2H), 7.56 (s, 1H), 7.44 (d, J = 8.0 Hz, 1H), 6.95 (s, 1H), 6.90 (d, J = 8.0 Hz, 1H), 6.69 (d, J = 8.0 Hz, 1H), 4.41 (d, J = 10.5 Hz, 1H), 4.27 (t, J = 5.5 Hz, 2H), 3.99 (t, J = 10.0 Hz, 1H), 3.19-3.13 (s, 1H), 3.04-2.99 (m, 1H), 2.94-2.90 (m, 1H), 2.68 (t, J = 5.5 Hz, 2H), 2.27 (s, 6H), 2.21 (s, 3H); ^{13}C NMR (125 MHz, DMSO-d_6) δ 171.21, 152.01, 150.55, 149.61, 146.94, 133.52, 130.49, 129.75, 129.45, 128.19, 122.39, 121.40, 121.22, 119.95, 116.38, 112.48, 67.72, 67.50, 57.94, 45.62, 31.73, 28.05, 20.57. IR (KBr, cm^{-1}): 2943, 1685, 1595, 1528, 1500, 1219, 1031, 811. HRMS calcd for $C_{26}H_{30}N_3O_3$: 432.2282 [M+H^+], found 432.2281.

*4.1.7. N-(2-(2-(Dimethylamino)ethoxy)-4-(pyridine-4-yl)phenyl)chromane-3-carboxamide(**7e**).*

White solid: 45% yield over four steps. Mp: 137-139°C. ^{1}H NMR (500 MHz, DMSO-d_6) δ 9.78 (NH, br, 1H), 8.61 (d, J = 4.5 Hz, 2H), 8.14 (d, J = 8.5 Hz, 1H), 7.75 (d, J = 5.5 Hz, 2H), 7.56 (s, 1H), 7.44 (d, J = 8.0 Hz, 1H), 7.15 (d, J = 7.5 Hz, 1H), 7.10 (t. J = 7.5 Hz, 1H), 6.87 (t, J = 7.0 Hz, 1H), 6.80 (d, J = 8.0 Hz, 1H), 4.45 (d, J = 10.5 Hz, 1H), 4.262 (t, J = 5.5 Hz, 2H), 4.03 (t, J = 10 Hz, 1H), 3.24-3.18 (m, 1H), 3.09-3.03 (m, 1H), 2.99-2.94 (m, 1H), 2.68 (t, J = 6.0 Hz, 2H), 2.26 (s, 6H); ^{13}C NMR (125 MHz, DMSO-d_6) δ 171.01, 154.19, 150.58, 149.72, 146.89, 133.62, 130.30, 129.85, 127.66, 122.52, 121.60, 121.39, 120.88, 120.04, 116.63, 112.87, 68.21, 67.54, 58.03, 45.82, 29.47, 28.13. IR (KBr, cm^{-1}): 2926, 1684, 1595, 1527, 1490, 1209, 1041, 811. HRMS calcd for $C_{25}H_{28}N_3O_3$: 418.2125 [M+H^+], found 418.2128.

*4.1.8. N-(2-(2-(Dimethylamino)ethoxy)-4-(pyridine-4-yl)phenyl)-6-chlorochromane-3-carboxamide(**7f**).*

Yellow solid: 38% yield over four steps. Mp: 105-107°C. ^{1}H NMR (500 MHz, DMSO-d_6) δ 9.77 (NH, br, 1H), 8.61 (s, 2H), 8.11 (d, J = 8.5 Hz, 1H), 7.75 (d, J = 5.5 Hz, 2H), 7.55 (s, 1H), 7.44 (d, J = 10.0 Hz, 1H), 7.24 (s, 1H), 7.13 (d, J = 6.0 Hz, 1H), 6.83 (d, J = 8.5 Hz, 1H), 4.45 (d, J = 11 Hz, 1H), 4.27 (t, J = 5.5 Hz, 2H), 4.07 (t, J = 10 Hz, 1H), 3.08-2.95 (m, 3H), 2.69 (t, J =

5.5 Hz, 2H), 2.27 (s, 6H); ^{13}C NMR (125 MHz, DMSO-d_6) δ 170.69, 153.10, 150.58, 149.73, 146.88, 133.68, 129.75, 129.63, 127.45, 124.39, 123.96, 122.55, 121.40, 120.03, 118.34, 112.86, 68.16, 67.78, 58.00, 45.80, 29.47, 27.80. IR (KBr, cm^{-1}): 2919, 1685, 1596, 1527, 1495, 1206, 1029, 811. HRMS calcd for $C_{25}H_{27}ClN_3O_3$: 452.1735 [M+H$^+$], found 452.1744.

*4.1.9. N-(2-(2-(Dimethylamino)ethoxy)-4-(pyridine-4-yl)phenyl)-6-fluorochromane-3-carboxamide(**7g**).*

Yellow solid: 40% yield over four steps. Mp: 101-103°C. ^{1}H NMR (500 MHz, DMSO-d_6) δ 9.73 (NH, br, 1H), 8.62 (s, 2H), 8.11 (d, J = 8.5 Hz, 1H), 7.75 (d, J = 5.0 Hz, 2H), 7.56 (s, 1H), 7.44 (d, J = 8.0 Hz, 1H), 7.03 (d, J = 9.0 Hz, 1H), 6.96-6.92 (m, 1H), 6.83-6.80 (m, 1H), 4.44 (d, J = 10.5 Hz, 1H), 4.27 (t, J = 5.5 Hz, 2H), 4.04 (t, J = 10 Hz, 1H), 3.23-3.16 (m, 1H), 3.09-3.04 (m, 1H), 3.00-2.95 (m, 1H), 2.68 (t, J = 5.5 Hz, 2H), 2.27 (s, 6H); ^{13}C NMR (125 MHz, DMSO-d_6) δ 170.77, 157.54, 155.67, 150.59, 150.46, 149.74, 146.87, 133.69, 129.81, 123.32, 123.26, 122.56, 121.40, 120.07, 117.78, 117.71, 116.14, 115.96, 114.41, 114.22, 112.99, 68.32, 67.71, 58.04, 45.88, 29.48, 28.02. IR (KBr, cm^{-1}): 2919, 1685, 1596, 1527, 1495, 1206, 1029, 811. HRMS calcd for $C_{25}H_{27}FN_3O_3$: 436.2031 [M+H$^+$], found 436.2030.

4.2. ROCK-1/2 Assays.[30,34]

Assays were performed using the STK2 kinase system from Cisbio. A 5 μL mixture of a 1μM STK2 substrate and ATP (ROCK1: 4 μM, ROCK2: 20μM) in STK-buffer was added to the wells of the 384-well plate using a BioRAPTR FRD Workstation (Aurora Discovery, Carlsbad, CA). Twenty nanoliters of test compound was then dispensed using a 384-head offline Pintool system (GNF System, San Diego, CA). The reaction was started by adding either 5μL of 2.5 nM ROCK1 (Upstate #14-601) or 5μL of 0.5 nM ROCK2 in STK-buffer. After 4h at RT the reaction was stopped by adding 10 μL of 1X antibody and 62.5 nM Sa-XL in Detection Buffer. After 1h incubation at RT, the plates were read on the Viewlux in HTRF mode.

4.3. Molecular docking

Molecular docking was performed using the Surflex-Dock module in Sybyl 2.0. Crystal structure of human ROCK1 (code: 2ETR) and human ROCK2 (code: 4L6Q) were downloaded from RCSB Protein Data Bank (http:/www.rcsb.org/pdb/home /home.do). The ligands were docked in the corresponding protein's binding site by an empirical scoring function and a patented search engine in Surflex-Dock. Before the docking process, the nature ligand was extracted and water molecules were removed from the crystal structure. Subsequently, the protein was prepared using Biopolymer module implemented in Sybyl. Then, a protocol was defined based on the original ligand. By default, 20 conformations were generated for each molecule and the conformation with best score was chosen for further studies.

4.4. Molecular dynamics (MD) simulations [35-40]

All preparation and production simulations were performed by AmberTools 14.0 package with the ff99SB force field for the kinase and general AMBER force field(gaff) for inhibitors. MD simulations follow the procedures of preparation, minimization, heating, balance, and production. Firstly, The complex system was simulated in a TIP3P water box environment. In this process, the SHAKE algorithm was applied to restraint stretching vibration of all bonds involving hydrogen atoms. The entire system suffered from energy minimization to eliminate possible space collisions with two steps. First step, the atom position of all solute species was restrained by the force of 100 kcal·mol^{-1}·Å^{-2}. Second step, the entire systems were optimized energy by 5000 steps of steepest descent method followed by 5000 steps of conjugated gradient method. Then the system was heated from 0 to 300K, followed by equilibration at 300K over 50 ps. Finally, a 10 ns production run was carried out by NPT ensemble at 300K with 1.013x10^5 kPa. All energy components were calculated using 50 snapshots extracted from 5 to 10 ns based on the RMSD results mentioned above.

At length, a production run for 10 ns under conditions of constant pressure and temperature was carried out. MD trajectories of all systems were taken to calculate the binding free energy with Molecular Mechanics/Generalized Born Surface Area (MM/GBSA) method reported by Onufiev (igb = 2).[41] In these calculations, the dielectric constants were set to 1.0 for the interior solute and 80.0 for the exterior solvent.

The contribution of residue to the total free energy was calculated by *sander* in *MMPBSA.py*.

Conflict of interest

The authors declare no conflict of interest.

Acknowledgments

Financial supports from National Natural Science Foundation of China (Grant No. 21502117), and the collaboration Innovation Foundation of Shanghai Institute of Technology, China (No.XTCX2016-3). We are also grateful to Prof. Gang Zhao and Prof. Guanjun Wang for technical assistance.

References and notes

1. Amano, M.; Nakayama, M.; Kaibuchi, K. Rho-kinase/ROCK: a key regulator of the cytoskeleton and cell polarity. *Cytoskeleton*. **2010**, *67*, 545-554.
2. Schmandke, A.; Schmandke, A.; Strittmatter, S. M.; ROCK and Rho: biochemistry and neuronal functions of Rho-associated protein kinases. *Neurosci*. **2007**, *13*, 454-469.
3. Mueller, B. K.; Mack, H. Teusch, N. Rho kinase, a promising drug target for neurological disorders. *Nat. Rev. Drug Discov*. **2005**, *4*, 387-398.
4. Shen, M. Y.; Tian, S.; Pan, P. C.; Sun, H. Y.; Li, D.; Li, Y. Y.; Zhou, H. F.; Li, C. W.; Lee, S.M.; Hou, T. J. Discovery of novel ROCK1 inhibitors via integrated virtual screening strategy and bioassays. *Sci. Rep.* **2015**, *5*, 16748.
5. Pan, P.C.; Shen, M. Y.; Yu, H. D.; Li, Y. Y.; Li, D.; Hou, T. J. Advances in the development of Rho-associated protein kinase (ROCK) inhibitors. *Drug Discov. Today* **2013**, *18*, 1323-1333.
6. Zhang, J. Y.; Dong, H. S.; Oqani R. K. Lin, T.; Kang, J. W.; Jin, D. Distinct roles of ROCK1 and ROCK2 during development of porcine preimplantation embryos. *Reproduction*. **2014**, *148*, 99-107.
7. Thumkeo, D.; Keel, J.; Ishizaki, T. Hirose, M.; Nonomura, K.; Oshima, H.; Oshima, M.; Taketo, M. M.; Narumiya, S. Targeted disruption of the mouse rho-associated kinase 2 gene results in intrauterine growth retardation and fetal death. *Mol. Cell. Biol.* **2003**, *23*, 5043-5055.
8. Shimizu, Y.; Thumkeo, D.; Keel, J. Ishizaki, T.; Oshima, H.; Oshima, M.; Noda, Y.; Matsumura, F.; Taketo, M. M.; Narumiya, S. ROCK-I regulates closure of the eyelids and ventral body wall by inducing assembly of actomyosin bundles. *J Cell Biol*. **2005**, *168*, 941-953.
9. Wen, X. J.; Wang, L. M.; ; Liu, Z. L.; Liu, Y. Y.; Hu, J. Y. Intracranial injection of PEG-PEI/ROCK II-siRNA improves cognitive impairment in a mouse model of Alzheimer's disease. *Int. J. Neurosci.* **2014**, *124*, 697-703.
10. Lane, R. F.; Small, S. A.; Gatson, J. W.; Ehrlich, M. E.; Gandy, S. Protein kinase C and rho activated coiled coil protein kinase 2 (ROCK2) modulate Alzheimer's APP metabolism and

phosphorylation of the Vps10-domain protein, SorL1. *Mol. Neurodegener.* **2010**, *5*, 62.
11. Liu, Y. Y.; Yang, X. Y.; Lei, Q. F.; Li, Z.; Hu, J. Y.; Wen, X. J.; Wang, H. J.; Liu, Z. L. PEG–PEI/siROCK2 protects against Aβ42-induced neurotoxicity in primary neuron cells for alzheimer disease. *Cell. Mol. Neurobiol.* **2015**, *35*, 841-848.
12. Saal, K. A.; Koch, J. C.; Tatenhorst, L.; Szego, E. M.; Ribas, V. T.; Michel, U.; Baehr, M.; Toenges, L.; Lingor, P. AAV. shRNA-mediated downregulation of ROCK2 attenuates degeneration of dopaminergic neurons in toxin-induced models of Parkinson's disease in vitro and in vivo. *Neurobiol. Dis.* **2015**, *73*, 150-162.
13. Liao, Y. C.; Liu, P. Y.; Lin, H. F.; Lin, W. Y.; Liao, J. K.; Juo, S. H. H. Two functional polymorphisms of ROCK2 enhance arterial stiffening through inhibiting its activity and expression. *J. Mol. Cell. Cardiol.* **2015**, *79*, 180-186.
14. Lee, J. H.; Zheng, Y.; von Bornstadt, D.; Wei, Y.; Balcioglu, A.; Daneshmand, A.; Yalcin. N.; Yu, E.; Herisson, F.; Atalay, Y. B.; Kim, M. H.; Ahn, Y. J.; Balkaya, M. Sweetnam, P.; Schueller, O.; Poyurovsky, M. V.; Kim, H. H.; Lo, E. H.; Furie, K. L.; Ayata, C. Selective ROCK2 inhibition in focal cerebral ischemia. *Ann. Clin. Transl. Neurol.* **2014**, *1*, 2-14.
15. Dyberg, C.; Fransson, S.; Andonova, T.; Sveinbjoernsson, B.; Laennerholm-Palm, J.; Olsen, T. K.; Forsberg, D.; Herlenius, E.; Martinsson, T.; Brodin, B.; Kogner, P.; Johnsen, J. I.; Wrickstroem, M. Rho-associated kinase is a therapeutic target in neuroblastoma. *Proc. Natl. Acad. Sci. U. S. A.* **2017**, *114*, E6603-E6612.
16. Shin, H. K.; Salomone, S.; Potts, E. M.; Lee, S. W.; Millican, E.; Noma, K.; Huang, P. L.; Boas, D. A.; Liao, J. K.; Moskowitz, M. A.; Ayata, C. Rho-kinase inhibition acutely augments blood flow in focal cerebral ischemia via endothelial mechanisms. *J. Cereb. Blood Flow Metab.* **2007**, *27*, 998-1009.
17. Nakagawa, O.; Fujisawa, K.; Ishizaki, T.; Saito, Y.; Nakao, K.; Narumiya, S. ROCK-I and ROCK-II, two isoforms of Rho-associated coiled-coil forming protein serine/threonine kinase in mice. *FEBS letters.* **1996**, *392*, 189-193.
18. Feng, Y.; LoGrasso, P. V.; Defert, O.; Li, R. S. Rho kinase (ROCK) inhibitors and their therapeutic potential. *J. Med. Chem.* **2015**, *59*, 2269-2300.
19. Zanin-Zhorov, A.; Weiss, J. M.; Nyuydzefe, M. S.; Chen, W.; Scher, J. U.; Mo, R.; Depoil, D.; Rao, N.; Liu, B.; Wei, J. L.; Lucas, S.; Koslow, M.; Roche, M.; Schueller, O.; Weiss, S.; Poyurovsky, M. V.; Tonra, J.; Hippen, K. L.; Dustin, M. L.; Blazar, B. R.; Liu, C. J.; Waksal S. D. Selective oral ROCK2 inhibitor down-regulates IL-21 and IL-17 secretion in human T cells via STAT3-dependent mechanism. *Proc. Natl. Acad. Sci.* **2014**, *111*, 16814-16819.
20. Pireddu, R.; Kara D. Forinash, K. D.; Sun, N. N.; Martin, M. P.; Sung, S. S.; Alexander, B.; Zhu, J. Y.; Guida, W. C.; Schonbrum, E. S.; Sebti, S. M.; Lawrence N. Pyridylthiazole-based ureas as inhibitor of Rho associted protein kinases (ROCK1 and 2). *Med. Chem. Commun.* **2012**, *3*, 699-709.
21. Li, R. S.; Martin, M. P.; Liu, Y.; Wang, B. L.; Ronil A. Patel, R. A.; Zhu, J. Y.; Sun, N.; Pireddu, R.; Lawrence, N. J.; Li, J. N.; Haura, E. B.; Sung, S. S.; Guid, W. C.; Schonbrunn, S.; Sebti S. M. Fragment-based and structure-guided discovery and optimization of Rho kinase inhibitors. *J. Med. Chem*. **2012**, *55*, 2474-2478.
22. Feng, Y. B.; Yin, Y.; Weiser, A.; Griffin, E.; Cameron, M. D.; Lin, L.; Ruiz, C.; Schurer, S. C.; Inoue, T.; Rao, P. V.; Schroter, T.; LoGrasso, P. Discovery of substituted 4-(pyrazol-4-yl)-phenylbenzodioxane-2-carboxamides as potent and highly selective Rho kinase (ROCK-II) inhibitors. *J. Med. Chem.* **2008**, *51*, 6642-6645.
23. Herskowitz, J. H.; Feng, Y. B.; Mattheyses, A. L.; Hales, C. M.; Higginbotham, L. A.; Duong, D. M.; Montine, T. J.; Troncoso, J. C.; Thambisetty, M.; Seyfried, N. T.; Levey, A. I.; Lah, J. Pharmacologic inhibition of ROCK2 suppresses amyloid-β production in an Alzheimer's disease mouse model. *J. Neurosci.* **2013**, *33*, 19086-19098.
24. Chen, Y. T.; Vojkovsky, T.; Fang, X. G.; Pocas, J. R.; Grant, W.; Handy, A. M. W.; Schroeter, T.; LoGrasso, P. Bannister, T. D.; Feng, Y. B. Asymmetric synthesis of potent chroman-based Rho kinase (ROCK-II) inhibitors. *MedChemComm*, **2011**, *2*, 73-75.
25. Grisar, J. M.; Marciniak, G.; Bolkenius, F. N.; Verne-mismer, J.; Wagner, E. R. Cardioselective Ammonium, Phosphonium, and Sulfonium Analogs of. alpha.-Tocopherol and Ascorbic Acid That Inhibit in Vitro and ex Vivo Lipid Peroxidation and Scavenge Superoxide Radicals. *J. Med. Chem.* **1995**, *38*, 2880-2886.
26. Loiodice, F.; Longo, A.; Bianco, P.; Tortorella, V. 6-Chloro-2, 3-dihydro-4H-1-benzopyran carboxylic acids: synthesis, optical resolution and absolute configuration. T*etrahedron: Asymmetry*, **1995**, *6*, 1001-1011.
27. Berardi, F.; Santoro, S.; Perrone, R.; Tortorella, V.; Govoni, S.; Lucchi, L. N-[ω-(Tetralin-1-yl) alkyl] derivatives of 3, 3-dimethylpiperidine are highly potent and selective σ1 or σ2 ligands. *J. Med. Chem.* **1998**, *41*, 3940-3947.
28. Chen, Y. T.; Bannister, T. D.; Weiser, A.; Griffin, E.; Lin, L.; Ruiz, C.; Cameron, M. D.; Schürer, S.; Duckett, D.; Schröter, T.; LoGrasso, P.; Feng Y. B. Chroman-3-amides as potent Rho kinase inhibitors. *Bioorg. Med. Chem. Lett.* **2008**, *18*, 6406–6409.
29. Noyori R. Asymmetric catalysis: Science and opportunities (Nobel lecture). *Angew. Chem. Int. Edition*. **2002**, *41*, 2008-2022.
30. Ding, M.; Yin, Y.; Wu, F. H.; Cui, J. X.; Zhou, H.; Sun, G. F.; Jiang, Y.; Feng, Y. B. Discovery of potent and selective urea-based ROCK inhibitors: Exploring the inhibitor's potency and ROCK2/PKA selectivity by 3D-QSAR, molecular docking and molecular dynamics simulations. *Bioorg. Med. Chem.* **2015**, *23*, 2505-2517.
31. Cui, J.; Ding, M.; Deng, W.; Yin, Y.; Wang, Z. H.; Zhou, H.; Sun, G. F.; Jiang, Y.; Feng, Y. B. Discovery of bis-aryl urea derivatives as potent and selective Limk inhibitors: Exploring Limk1 activity and Limk1/ROCK2 selectivity through a combined computational study. *Bioorg. Med. Chem*. **2015**, *23*, 7464-7477.
32. Shen, M. Y.; Zhou, S. Y.; Li, Y. Y.; Pan, P. C.; Zhang, L. L.; Hou, T. J. Discovery and optimization of triazine derivatives as ROCK1 inhibitors: molecular docking, molecular dynamics simulations and free energy calculations. *Mol. BioSyst.* **2013**, *9*, 361-374.
33. Karami L, Saboury A. A.; Rezaee E.; Tabatabai, S. A. Investigation of the binding mode of 1, 3, 4-oxadiazole derivatives as amide-based inhibitors for soluble epoxide hydrolase (sEH) by molecular docking and MM-GBSA. *Eur. Biophys.J.* **2017**, *46*, 445-459.
34. Yin, Y.; Cameron, M. D.; Lin, L.; Khan, S.; Schroter, T.; Grant, W.; Pocas, J.; Chen, Y. T.; Schrurer, S.; Pachori, A.; LoGrasso, P.; Feng, Y. B. Discovery of potent and selective urea-based ROCK inhibitors and their effects on intraocular pressure in rats. *Acs Med. Chem. Lett*. **2010**, *1*, 175-179.
35. Sun, H. Y.; Duan, L. L.; Chen, F.; Liu, H.; Wang, Z.; Pan, P. C.; Zhu, F.; Zhang, Z. H.; Hou, T. J. Assessing the performance of MM/PBSA and MM/GBSA methods. 7. Entropy effects on the performance of end-point binding free energy calculation approaches. *Phys. Chem. Chem. Phys.* **2018**, *20*, 14450-14460.
36. Chen, F.; Liu, H.; Sun, H. Y.; Pan, P. C.; Li, Y. Y.; Li, D.; Hou, T. J. Assessing the performance of MM/PBSA and MM/GBSA methods. 6. Capability to predict protein-protein binding free energies and re-rank binding poses generated by protein-protein docking. *Phys. Chem. Chem. Phys.* **2016**, *18*, 22129-22139.
37. Sun, H. Y.; Li, Y. Y.; Shen, M. Y.; Tian, S.; Xu, L.; Pan, P. C.; Guan, Y.; Hou, T. J. Assessing the performance of MM/PBSA and MM/GBSA methods. 5. Improved docking performance by using high solute dielectric constant MM/GBSA and MM/PBSA rescoring. *Phys. Chem. Chem. Phys.* **2014**, *16*, 22035-22045.
38. Sun, H. Y.; Li, Y. Y.; Tian, S.; Xu, L.; Hou, T. J. Assessing the performance of MM/PBSA and MM/GBSA methods. 4. Accuracies of MM/PBSA and MM/GBSA methodologies evaluated by various simulation protocols using PDBbind data set. *Phys. Chem. Chem. Phys.* **2014**, *16*, 16719-16729.
39. Hou, T. J.; Wang, J. M.; Li, Y. Y.; Wang, W. Assessing the performance of the molecular mechanics/poisson boltzmann surface area and molecular mechanics/Generalized born surface area methods. II. The accuracy of ranking poses generated from docking. *J. Comput. Chem.* **2011**, *32*, 866-877.
40. Hou, T. J.; Wang, J. M.; Li, Y. Y.; Wang, W. Assessing the performance of the MM/PBSA and MM/GBSA methods. I. The accuracy of binding free energy calculation based on molecular dynamics simulations. *J. Chem. Inf. Model.* **2011**, *51*, 69-82.
41. Onufriev, A.; Bashford, D.; Care, D. A. Modification of the generalized born model suitable for macromolecules. *J. Phys. Chem. B* **2000**, *104*, 3712-3720.

Supplementary Material

Supplementary data associated with this article can be found, in the online version, at https://doi.org/

Click here to remove instruction text...